Time-Optimal Trajectories to Circumsolar Space Using Solar Electric Propulsion

Alessandro A. Quarta, [a,*] Dario Izzo, [b] and Massimiliano Vasile [c]

[a] *Dipartimento di Ingegneria Aerospaziale, University of Pisa, I-56122 Pisa, Italy*

[b] *Advanced Concepts Team, European Space Agency, Noordwijk, The Netherlands*

[c] *Department of Mechanical Engineering, University of Strathclyde, Glasgow, UK*

Abstract

The aim of this paper is to explore the capabilities of a solar electric propelled spacecraft on a mission towards circumsolar space. Using an indirect approach, the paper investigates minimum time of transfer (direct) trajectories from an initial heliocentric parking orbit to a desired final heliocentric target orbit, with a low perihelion radius and a high orbital inclination. The simulation results are then collected into graphs and tables for a trade-off analysis of the main mission parameters. Finally, a comparison of the performance between a solar electric and a (photonic) solar sail based spacecraft is discussed.

Key words: Minimum time trajectories ; Solar electric propulsion ; Circumsolar space exploration

* Corresponding author.

Email addresses: a.quarta@ing.unipi.it (Alessandro A. Quarta,), dario.izzo@esa.int (Dario Izzo,), massimiliano.vasile@strath.ac.uk (Massimiliano Vasile).

Nomenclature

$\mathbb{A}$	=	matrix $\in \mathbb{R}^{7\times 3}$, see Eq. (2)
A	=	sail reflective area
a	=	semimajor axis
a_c	=	solar sail characteristic acceleration
$\hat{\boldsymbol{a}}_T$	=	propulsive acceleration unit vector
$\boldsymbol{d}$	=	vector $\in \mathbb{R}^{7\times 1}$, see Eq. (3)
e	=	orbital eccentricity
f, g, h, k	=	modified equinoctial elements
H	=	Hamiltonian function
i	=	orbital inclination
I_d	=	electric thruster operation point
J	=	performance index
L	=	true longitude
m	=	spacecraft mass
P	=	input power to Power Processing Unit
$\mathcal{P}$	=	solar radiation pressure at 1 AU
P_L	=	payload power
$P_\oplus$	=	solar array initial output power
p	=	semilatus rectum
r	=	Sun-spacecraft distance
r_a	=	target orbit's aphelion radius
r_p	=	target orbit's perihelion radius
T	=	electric thruster's propulsive thrust
t	=	time

$\boldsymbol{x}$	=	state vector
β	=	propellant mass flow rate
δ	=	ecliptic declination
η_P	=	duty cycle
$\boldsymbol{\lambda}$	=	adjoint vector
λ	=	adjoint variable
$\mu_\odot$	=	Sun's gravitational parameter
ν	=	true anomaly
ω	=	argument of perihelion
Ω	=	right ascension of the ascending node
σ_{sa}	=	sail assembly loading

Subscripts

0	=	initial, injected, parking orbit
1	=	final, target orbit
p	=	propellant
pay	=	payload
sa	=	sail assembly

Superscripts

$\cdot$	=	time derivative

1 Introduction

The circumsolar space, with particular reference to the region around the Sun's poles, is still, to a large extent, an unexplored part of our Solar System. Despite a continuous progress of remote sensing capabilities, a deep knowledge of the inner heliosphere can be obtained only through accurate in-situ measurements (Heliophysics Roadmap Team, 2009). In fact, an in-depth analysis of the solar wind or a thorough measurement of the solar magnetic field, and of its interaction with the external corona, requires the use (in situ) of a scientific probe. Even more interesting is the possibility to observe the Sun at high inclinations above the Ecliptic plane.

The interest of the scientific community for exploring the circumsolar space has been revived after the remarkable results of the Ulysses mission, including the observation of an unexplained constant decrease of the solar wind since the beginning of space based recordings, and further confirmed by the launch of the European probe Solar Orbiter (ESA Study Scientists, 2011), which is scheduled for the beginning of 2017. Its operating orbit is characterized by a perihelion distance of about 0.28 AU and an inclination greater than 25 deg with respect to the solar equatorial plane. Such a probe is expected to provide detailed information both of the inner heliosphere and of the solar polar regions. A closer view of the Sun will be given by the American Solar Probe Plus (APL Team, 2008), whose launch will take place on 2018. The Solar Probe Plus should be the first spacecraft capable of traveling within the solar atmosphere (the solar corona) and reaching a distance of 5.9 million kilometers (that is, 8.5 solar radii) from the photosphere, the region from which the photons originate.

The difficulty of reaching the circumsolar space with a scientific probe comes from the high ΔV necessary for those mission types. In fact, the desired scientific measurements typically require the achievement of a heliocentric orbit with a low perihelion and a high inclination with respect

to the Ecliptic plane. For example, a circular orbit with a radius of 0.28 AU and an inclination of 28 deg with respect to the Ecliptic plane would require a minimum $\Delta V \simeq 29\,\mathrm{km/s}$ using a two impulse maneuver. Such a value could be reduced, the perihelion distance and inclination being the same, using an elliptic orbit. In fact, with an aphelion radius of 0.8 AU the ΔV decreases to about 17.2 km/s. The Ulysses mission, one of the very first missions dedicated to watch the Sun closely, acquired an orbit inclination of 80 deg while retaining a perihelion radius larger than 1 AU. The spacecraft left the Earth with a staggering speed of 15.7 km/s, making it, at that time, the fastest interplanetary spacecraft ever launched. Such a high speed was the price to be paid to reach Jupiter and pump up there the inclination for free, which also forced the orbit aphelion to be at roughly 5 AU.

The remarkably high values of ΔV that characterize space missions (also referred to as "high energy" missions) towards the circumsolar space, usually require a high hyperbolic excess velocity at launch and multiple gravity assist maneuvers to reduce the propellant consumption within acceptable limits. For example, the Solar Probe Plus mission plans seven flybys with Venus, while the Solar Orbiter mission schedules two flybys with Earth in addition to several Venus gravity assists.

Clearly, the presence of multiple flybys makes the transfer trajectory design more difficult and introduces constraints on the launch windows. On the other side, a direct transfer, which could offer a higher flexibility on launch windows, would be impossible for a (chemical) high thrust propulsion system, due to an excessively high value of ΔV. Not surprisingly, missions towards the heliosphere have been studied using innovative propulsion systems like solar sails (Sauer, 1999). Indeed, solar sails are particulary suitable for transfers in the inner Solar System as the propulsive force they generate is proportional to the local solar flux, which in turns varies with the inverse square distance from the Sun. Note that, in a solar-powered spacecraft in which the electric power is supplied by solar arrays, the maximum input power (and then the propulsive thrust) is an involved function of the distance from the Sun (Rayman and Williams, 2002),

but also depends on the flight time due to the solar cells degradation (Saleh et al., 2002).

However, despite the recent successes of the Japanese IKAROS mission (Tsuda et al., 2011), which first used a solar sail for an interplanetary mission, this kind of propulsion system does not yet offer a satisfactory technology readiness level (Johnson et al., 2010). A possible alternative, which currently guarantees a greater confidence level, is given by solar electric propulsion (SEP) technology (Brophy and Noca, 1998; Circi, 2003). As is well known, the high specific impulse provided by SEP systems allows for a significant reduction of the propellant necessary to complete the transfer (Williams and Coverstone-Carroll, 1997). Current space missions designed to reach the inner part of the Solar System with SEP technology, use solar electric propulsion in combination with multiple gravity assists to maximize the payload mass delivered into the final operational orbit. Examples are the initial design of the Solar Orbiter mission (Vasile and Bernelli-Zazzera, 2003b) or the design of the BepiColombo mission (Vasile and Bernelli-Zazzera, 2003a). Furthermore, future concepts envisage the use of these propulsion systems in conjunction with a solar sail, thus constituting a hybrid solution (Leipold and Götz, 2002; Mengali and Quarta, 2007) that seeks to overcome the intrinsic limitations of the each system alone (Circi, 2004; Macdonald and McInnes, 2011).

In any case, an assessment of the performance of a pure SEP system for a direct transfer is useful to evaluate the possible improvements provided by a hybrid solution, or by the inclusion of gravity assist maneuvers. This paper addresses a preliminary performance investigation for a spacecraft equipped with a SEP propulsion system, whose aim is to reach the circumsolar space. The study takes into account the actual performance of a SEP system of last generation. Minimum time trajectories necessary to obtain a direct transfer towards a target orbit with prescribed characteristics are found using an indirect approach based on optimal control theory. The rationale is that a minimum time trajectory provides an upper limit on the propellant mass along a possible optimal time vs. mass trade-off curve for a direct transfer. In other words any other optimal direct transfer solution that aims at minimizing the mass of propellant will

have a longer transfer time.

2 Mathematical Model

The equations of motion (Betts, 2000) of a SEP spacecraft, in a heliocentric inertial reference frame, may be expressed in terms of Modified Equinoctial Orbital Elements (Walker et al., 1985; Walker, 1986) (MEOE) p, f, g, h, k, and L as:

$$\dot{\boldsymbol{x}} = \eta_P \, (T/m) \, \mathbb{A} \, \hat{\boldsymbol{a}}_T + \boldsymbol{d} \tag{1}$$

where $\boldsymbol{x} \triangleq [p,\, f,\, g,\, h,\, k,\, L, m]^{\mathrm{T}}$ is the state vector, m is the spacecraft mass, $T \geq 0$ is the propulsive thrust modulus, $\hat{\boldsymbol{a}}_T$ is the thrust unit vector whose components are expressed in a local-vertical/local-horizontal orbital reference frame, and $\eta_P = 0.92$ is the duty cycle. The latter, according to Rayman and Williams (2002), is the fraction of time during deterministic thrust periods in which $T \neq 0$. In Eq. (1), $\mathbb{A} \in \mathbb{R}^{7\times 3}$ is a matrix in the form:

$$\mathbb{A} \triangleq \sqrt{\frac{p}{\mu_\odot}} \begin{bmatrix} 0 & \left[\dfrac{2\,p}{1+f\,\cos L+g\,\sin L}\right] & 0 \\ [\sin L] & \left[\dfrac{(2+f\,\cos L+g\,\sin L)\,\cos L+f}{1+f\,\cos L+g\,\sin L}\right] & \left[-\dfrac{g\,(h\,\sin L-k\,\cos L)}{1+f\,\cos L+g\,\sin L}\right] \\ [-\cos L] & \left[\dfrac{(2+f\,\cos L+g\,\sin L)\,\sin L+g}{1+f\,\cos L+g\,\sin L}\right] & \left[\dfrac{f\,(h\,\sin L-k\,\cos L)}{1+f\,\cos L+g\,\sin L}\right] \\ 0 & 0 & \left[\dfrac{(1+h^2+k^2)\,\cos L}{2\,(1+f\,\cos L+g\,\sin L)}\right] \\ 0 & 0 & \left[\dfrac{(1+h^2+k^2)\,\sin L}{2\,(1+f\,\cos L+g\,\sin L)}\right] \\ 0 & 0 & \left[\dfrac{h\,\sin L-k\,\cos L}{1+f\,\cos L+g\,\sin L}\right] \\ 0 & 0 & 0 \end{bmatrix} \tag{2}$$

where $\mu_\odot \triangleq 132\,712\,439\,935.5\,\mathrm{km}^3/\mathrm{s}^2$ is the Sun's gravitational parameter, and the vector $\boldsymbol{d} \in \mathbb{R}^{7\times 1}$ is defined as

$$\boldsymbol{d} \triangleq \left[0,\, 0,\, 0,\, 0,\, 0,\, \sqrt{\mu_\odot\, p}\, \left(\frac{1 + f\, \cos L + g\, \sin L}{p}\right)^2, -\eta_P\, \beta\right]^{\mathrm{T}} \tag{3}$$

where $\beta \geq 0$ is the propellant mass flow rate. Note that p is the semilatus rectum of the spacecraft osculating orbit, whereas the transformations from MEOE to the classical orbital elements are

$$a = \frac{p}{1 - f^2 - g^2} \tag{4}$$

$$e = \sqrt{f^2 + g^2} \tag{5}$$

$$i = 2\, \arctan \sqrt{h^2 + k^2} \tag{6}$$

$$\sin\omega = g\, h - f\, k \quad , \quad \cos\omega = f\, h + g\, k \tag{7}$$

$$\sin\Omega = k \quad , \quad \cos\Omega = h \tag{8}$$

$$\nu = L - \Omega - \omega \tag{9}$$

where a is the semimajor axis, e is the eccentricity, i the orbital inclination, ω is the argument of perihelion, Ω is the longitude of the ascending node, and ν is the true anomaly of the spacecraft's osculating orbit.

In a SEP spacecraft, the thrust level T and the propellant mass flow rate β are closely related to the input power P to the Power Processing Unit (PPU). In particular, an electric thruster has a finite number of operation points (Patterson et al., 2001; Patterson and Benson, 2007), each one characterized by a corresponding set of values of T, β, and P. If the propulsion system performance coincides with that of a NASA's Evolutionary Xenon Thruster (NEXT)

ion thruster (Patterson and Benson, 2007), a set of 40 operation points (or I_d) is available, see Fig. 1. In the simulations, a fictitious operation point (that is $I_d = 41$, where $T = 0$ and $\beta = 0$) has been added to the actual NEXT thrust table, to model the presence of possible coasting phases in the spacecraft optimal trajectory. Therefore, within this simplified model, the operation point $I_d \in \mathbb{N}^+$ (with $I_d \leq 41$), represents the only control parameter that describes the thruster performance in terms of T and β.

For example, when the first operation point $I_d = 1$ is selected, the propulsion system supplies the maximum thrust (about 0.236 N) at the maximum propellant mass flow rate (about 5.76 mg/s), see Fig. 1. Note that the condition $I_d = 1$ can be selected only if the PPU input power is (at least) 7.22 kW. In fact, assuming a photovoltaic power generation system with degradation effects (Rayman and Williams, 2002; Oh, 2007), the set of all admissible operation points is strictly related to the available input power. The latter is defined as the difference of the solar array output power and the power allocated to operate the spacecraft systems $P_L \triangleq 400$ W. Therefore, when an initial output power $P_\oplus$ is given, the set of admissible operation points depends both on the Sun-spacecraft distance and the time (Rayman and Williams, 2002). The mathematical model and the flow diagram of the electric power calculation are discussed in Quarta and Mengali (2011). In this paper $P_\oplus$ is chosen to coincide with the solar array output power at the beginning of the mission, and at a reference Sun-spacecraft distance equal to 1 AU.

2.1 Trajectory optimization

Assume that the initial (corresponding to $t_0 \triangleq 0$) spacecraft osculating orbit coincides with the Earth's (Keplerian) heliocentric orbit, viz.

$$p(t_0) = 9.9878 \times 10^{-1}\,\mathrm{AU} \quad , \quad f(t_0) = -3.5778 \times 10^{-3} \quad , \quad g(t_0) = 1.5344 \times 10^{-2}$$
$$h(t_0) = -1.5181 \times 10^{-5} \quad , \quad k(t_0) = 2.1250 \times 10^{-5} \tag{10}$$

This scenario is representative of a spacecraft injection on a parabolic Earth escape trajectory, with zero hyperbolic excess energy with respect to the planet.

The optimization problem consists of finding the minimum time trajectory that transfers the spacecraft from the initial orbit to a final (prescribed) target orbit. This amounts to maximizing the objective function $J \triangleq -t_1$, where t_1 is the total flight time. Using an indirect approach (Betts, 1998), the optimal thrust direction $\hat{\boldsymbol{a}}_T$ is obtained through Pontryagin's maximum principle (Chobotov, 1996) as

$$\hat{\boldsymbol{a}}_T = \frac{\mathbb{A}^{\mathrm{T}}\,\boldsymbol{\lambda}}{\|\mathbb{A}^{\mathrm{T}}\,\boldsymbol{\lambda}\|} \tag{11}$$

where $\boldsymbol{\lambda} \in \mathbb{R}^{7\times 1}$ is the adjoint vector

$$\boldsymbol{\lambda} \triangleq [\lambda_p,\, \lambda_f,\, \lambda_g,\, \lambda_h,\, \lambda_k,\, \lambda_L,\, \lambda_m]^{\mathrm{T}} \tag{12}$$

whose time derivative is given by the Euler-Lagrange equations

$$\dot{\boldsymbol{\lambda}} = -\frac{\partial H}{\partial \boldsymbol{x}} \tag{13}$$

where $H \triangleq [\eta_P\,(T/m)\,\mathbb{A}\,\hat{\boldsymbol{a}}_T \cdot \boldsymbol{\lambda} + \boldsymbol{d} \cdot \boldsymbol{\lambda}]$ is the Hamiltonian function. The explicit expressions of

the Euler-Lagrange equations, evaluated using a symbolic math toolbox, has been omitted for the sake of brevity. According to Quarta and Mengali (2011), the optimal thrust level T (and so the propellant mass flow rate β) is obtained, using a numerical approach (Hoare, 1962), by maximizing the Hamiltonian function H with respect to I_d. Note that the maximization process of H should take into account the constraint condition on the actual value of the available power for the propulsion system.

The spacecraft motion is described by the seven equations of motion (1) and the seven Euler-Lagrange equations (13). This differential system must be completed with 14 suitable boundary conditions, the first five of these are shown in Eq. (10). Because the initial spacecraft angular position is left free, the initial true longitude $L(t_0)$ is an output of the optimization process. The sixth boundary condition refers to the initial (given) spacecraft mass $m_0 \triangleq m(t_0)$, whereas the remaining eight conditions (along with the minimum flight time t_1) are obtained by enforcing the transversality condition (Bryson and Ho, 1975), following the procedure described in Casalino et al. (1998, 1999). In particular, when the inclination i_1, the perihelion radius r_p, and the aphelion radius r_a of the heliocentric target orbit are all fixed, Eqs. (5) and (6) provide the following three constraints on the final value (subscript 1) of MEOE:

$$i_1 = 2 \arctan \sqrt{h_1^2 + k_1^2} \quad , \quad \frac{r_a - r_p}{r_a + r_p} = \sqrt{f_1^2 + g_1^2} \quad , \quad p_1 = \frac{2\, r_p\, r_a}{r_p + r_a} \tag{14}$$

A set of heliocentric canonical units (Bate et al., 1971), in which the spacecraft injected mass m_0 coincides with the mass unit, has been used in the integration of the differential equations to reduce their numerical sensitivity. The equations of motion (1) and the Euler-Lagrange equations (13) have been integrated in double precision using a variable order Adams-Bashforth-Moulton solver scheme (Shampine and Gordon, 1975) with absolute and relative errors of 10^{-12}. Finally, the boundary-value problem associated to the variational problem has been solved through a hybrid numerical technique that combines genetic algorithms (to obtain a first estimate of

adjoint variables), with gradient-based and direct methods to refine the solution.

3 Problem Description and Simulations Results

Assume that the spacecraft, with an injected mass m_0, is equipped with a SEP system, whose performance model is based on that of the NEXT thruster. The problem is to find the minimum time, direct trajectory (that is, without gravity assist maneuvers) that transfers the spacecraft from an Earth's heliocentric orbit to a Keplerian target orbit, under the assumption that perihelion radius r_p, aphelion radius r_a and orbital inclination i_1, are all given, see Eqs. (14). The optimization problem is solved by means of the indirect approach described in the previous section. Note that, in all of the simulations, the initial ν_0 and final ν_1 spacecraft true anomaly, the final spacecraft mass m_1, the target orbit's argument of perihelion ω_1, and the right ascension of the ascending node Ω_1, are all left free. Their optimal values are therefore obtained as outputs of the optimization process.

For a given target orbit characteristics, that is, for a given set of values (r_p, r_a, i_1), the minimum flight time t_1 is a function of both the injected mass m_0 and the initial solar array output power $P_\oplus$. Equivalently, in mathematical terms, the flight time may be expressed as $t_1 = t_1\,(r_p,\, r_a,\, i_1,\, m_0,\, P_\oplus)$. For example, assume that $m_0 = 1000\,\mathrm{kg}$, $P_\oplus = 10\,\mathrm{kW}$, and that the target orbit characteristics are $r_p = 0.3\,\mathrm{AU}$, $r_a = 0.8\,\mathrm{AU}$ and $i_1 = 24\,\mathrm{deg}$. These data are consistent with the Solar Orbiter operational orbit (ESA Study Scientists, 2011). The optimization process provides a minimum flight time $t_1 = 952.9\,\mathrm{days}$, whereas the propellant consumption is $m_p \triangleq m_0 - m_1 \simeq 436.3\,\mathrm{kg}$ (the propellant mass fraction is $m_p/m_0 = 43.6\%$). The corresponding transfer trajectory is shown in Fig. 2, where the asterisk denotes the perihelion of the parking and target orbit, whereas the circle refers to the starting (or arrival) point.

The heliocentric transfer starts when the spacecraft initial true anomaly is $\nu_0 \simeq 136\,\text{deg}$, as is shown in Fig. 2(a), and ends when the spacecraft completes approximately four revolutions around the Sun. Note that the departure orbit coincides, by construction, with the Earth's heliocentric orbit (see Eq. (10)), and therefore an optimal launch opportunity occurs (yearly) on May 20.

Figures 3 and 4 show the variation of the semimajor axis a, inclination i, perihelion $p/(1+e)$ and aphelion $p/(1-e)$ radius of the osculating orbit along the optimal transfer trajectory. In particular, Fig. 3 shows that the orbital inclination changes mainly at aphelion passages (which are placed close to the nodes), and the aphelion radius is initially increased to improve the propulsive acceleration effectiveness in the plane change maneuver. Unlike locally optimal steering laws (Macdonald and McInnes, 2005), a non-monotonic time-variation of the osculating orbit elements and characteristics (such as aphelion and perihelion) is typical of truly optimal control laws, even though this does not constitute a proof of the global optimality of the performance index (in this case the total flight time). Such a behavior is consistent with what was observed by Dachwald et al. (2006b) in a similar mission scenario, where a near-term solar sail reaches an heliocentric orbit with a low perihelion radius and a high inclination.

Figure 5 shows the time variation of the Sun-spacecraft distance r and the spacecraft (ecliptic) declination δ during the time-optimal transfer. Note that δ is the angle between the Sun-spacecraft line and the Ecliptic plane. Figure 5 also shows that the local maxima of $r = r(t)$ are all located in the neighboring of the Ecliptic plane ($\delta = 0$).

3.1 Sensitivity analysis

A sensitivity analysis of mission performance, obtained by varying the injected mass in the range $m_0 \in [550,\, 1350]\,\text{kg}$ and the initial solar array output power in the interval $P_\oplus \in$

[5.5, 10] kW, is now presented. Note that a variation of $P_{\oplus}$ with respect to the reference value (of 10 kilowatts) may reasonably be used to model a (partial) failure of the solar electric power system. The simulation results are summarized in Tables 1 and 2. When the initial electric power $P_{\oplus}$ is kept fixed, and injected mass m_0 is varied within the selected range, the propellant mass fraction m_p/m_0 displays a small fluctuation around a mean value of about 43.21%, see the third column of Table 1. This corresponds roughly to a linear variation of the propellant mass m_p versus the spacecraft injected mass m_0, in the selected range. A similar conclusion holds true for the minimum flight time t_1 versus m_0, which may be approximated as

$$t_1 \simeq 0.9479\, m_0 \tag{15}$$

where t_1 is expressed in days and m_0 in kilograms.

Note that the propellant throughput capability of a NEXT propulsion system (Van Noord, 2007) is about 450 kg (qualification-level), which corresponds to 22000 hours of operation at maximum thrust (operation point $I_d = 1$, see Fig. 1). Therefore, according to Table 1, only the mission scenario in which $m_0 \leq 1050$ kg is consistent with the actual characteristics of a single propulsive unit. Table 1 also shows that, when $m_0 = 1050$ kg, the spacecraft dry mass is less than $m_1 \simeq 600$ kg, a value consistent with those reported in Table 2 of Oh et al. (2008) for a rendezvous mission towards comet Tempel 1 of a SEP spacecraft with a NEXT thruster and $P_{\oplus} = 10$ kW. However, laboratory tests (Herman et al., 2009; Reckart, 2009) indicate that the NEXT thruster could (potentially) provide a propellant throughput greater than 750 kg, and this enhanced capability would make other mission scenarios possible.

For a given injected mass m_0, the propellant mass fraction m_p/m_0 is affected by the value of $P_{\oplus}$, see the third column of Table 2. This behavior is closely related to the propulsion system mathematical model. In fact, as the simulations show, the optimal thrusting strategy consists of selecting (at any time) the maximum propulsive thrust. If the available power is always greater

than 7.22 kW, then the thruster operation point is $I_d = 1$ along the whole transfer trajectory. This explains why a initial power $P_\oplus \geq 9.5\,\text{kW}$ gives the same mission performance, see the last two rows in Table 2. However, when the available power becomes less than 7.22 kW, because either the spacecraft is too far from the Sun or the value of $P_\oplus$ is insufficient, the optimization process selects an operation point different from $I_d = 1$. This situation is illustrated in Figure 6, where the time history of the thruster operation point I_d is shown as a function of $P_\oplus$. Note, from Table 2, that there is a little difference in performances between the case of $P_\oplus = 7\,\text{kW}$ and $P_\oplus = 7.5\,\text{kW}$. In other terms, the value $P_\oplus \simeq 7\,\text{kW}$ is suboptimal in this mission scenario.

The flight time and the propellant mass fraction depend on the target orbit characteristics. For example Tables 3 and 4 show the mission performance as a function of $i_1 \in [0,\, 30]\,\text{deg}$ and $r_a \in [0.3,\, 1]\,\text{AU}$, respectively. In particular, the case of $i_1 = 0$ corresponds to a two-dimensional transfer towards an elliptic target orbit with perihelion radius $r_p = 0.3\,\text{AU}$ and aphelion radius $r_a = 0.8\,\text{AU}$. The case of $r_a = 0.3\,\text{AU}$, instead, corresponds to an optimal transfer towards a circular heliocentric orbit with inclination $i_1 = 24\,\text{deg}$, see Fig. 7 for the spacecraft's trajectory.

3.2 Comparison with an ideal solar sail

A comparison of the performance of a SEP spacecraft with a vehicle equipped with an advanced, propellantless, propulsion system, such as a (photonic) solar sail, is briefly discussed in this section. Note that a thorough comparison between two different propulsion systems is a very complex task and, in this respect, the following analysis does not intend to provide a conclusive indication on which type of propulsion system is best for the type of missions considered in this paper. Instead, this simplified comparison aims at highlighting some of the technological requirements and potentialities of the two propulsion systems in the context of circumsolar missions.

The comparison between the performance of a SEP and a solar sail spacecraft can be made by taking into account different performance indexes as, for example, the mission flight time, the payload mass, or the payload mass fraction. In this analysis, the payload for a solar sail based spacecraft should be intended as the vehicle that will perform the science operations at the given target orbit (Macdonald et al., 2006).

Instead, in this comparison, the flight time of the sail spacecraft is fixed to the one required to the SEP spacecraft, and the characteristic acceleration of the solar sail a_c is minimized using an optimization algorithm, adapted from Mengali and Quarta (2009). Recall that a_c is defined (McInnes, 1999) as the maximum solar sail propulsive acceleration when the Sun-spacecraft distance is 1 AU.

Introduce now a simplified solar sail mass breakdown model, where the total spacecraft mass m_0 is the sum of the payload mass m_{pay}, and the sail assembly mass m_{sa}. Recall that the sail assembly mass includes the mass of both the reflective film, and the required structure for storing, deploying and tensioning the sail (Dachwald, 2004). Consider an ideal flat solar sail force model without degradation (Dachwald et al., 2006a, 2007), that is a sail with a perfectly reflecting film. For a given payload mass fraction m_{pay}/m_0, the sail assembly loading σ_{sa} is related to the solar sail characteristic acceleration a_c through the simple equation

$$\sigma_{\text{sa}} = \frac{2\,\mathcal{P}\,(1 - m_{\text{pay}}/m_0)}{a_c} \tag{16}$$

where $\mathcal{P} \triangleq 4.56 \times 10^{-6}\,\text{N/m}^2$ is the solar radiation pressure at a distance of 1 AU from the Sun. In Eq. (16), the sail assembly loading $\sigma_{\text{sa}} \triangleq m_{\text{sa}}/A$, usually measured in grams per square meter, is defined as the ratio between the sail assembly mass m_{sa} and the sail reflective area A. According to Dachwald (2005), σ_{sa} is the key parameter for the efficiency of the solar sail's structural design. In particular, a goal value of the sail assembly loading for an advanced, near-term, solar sail is about $10\,\text{g/m}^2$. Currently, realistic values of σ_{sa} are on the order of

$25 - 30\,\mathrm{g/m^2}$ (Ceriotti, 2011).

When a ideal solar sail is considered in the trajectory simulations, the (minimum) values of the characteristic acceleration shown in the second last column of Tabs. 1–4 are obtained. For example, the simulations show that an ideal solar sail with a characteristic acceleration $a_c \simeq 0.375\,\mathrm{mm/s^2}$, could perform a transfer towards a target orbit with $r_p = 0.3\,\mathrm{AU}$, $r_a = 0.8\,\mathrm{AU}$, and $i_1 = 24\,\mathrm{deg}$, in about 1000 days, see Tab. 1. The same mission can be completed by a SEP spacecraft, using a realistic propulsion system, with a final mass fraction of about 56.47%. From the definition of sail characteristic acceleration in Eq. (16), one can derive, for the same mass fraction, an assembly loading of about $10.6\,\mathrm{g/m^2}$. In other terms, this mission scenario requires an advanced, near-term solar sail in order to release, on the operational orbit, the same final mass fraction of a SEP spacecraft.

Note, however, that the value of the sail loading is not conservative, because an ideal sail force model was used in the simulations. If a realistic sail force model (that is, a model that consider both the sail film optical properties and the sail actual shape) was considered, the value of the required sail assembly loading would decrease with respect to the ideal case. Of course, the value of the (corresponding) sail assembly loading changes with the total flight time and the mission scenario, as shown in the last column of Tabs. 1–4.

Finally, taking into account that for a given target orbit $a_c = a_c(t_1)$ is a monotonic decreasing function, it is noteworthy to observe that the discussed results are consistent with those of an optimization analysis in which both the flight time is minimized and the sail characteristic acceleration is fixed. In other terms, in a mission scenario in which a flat, ideal, solar sail of characteristic acceleration $a_c \simeq 0.375\,\mathrm{mm/s^2}$ reaches a target orbit with $r_p = 0.3\,\mathrm{AU}$, $r_a = 0.8\,\mathrm{AU}$, and $i_1 = 24\,\mathrm{deg}$, the minimum flight time is indeed $t_1 = 1000\,\mathrm{days}$.

4 Conclusions

The design of high-energy space physics missions offer the intriguing opportunity to explore the capabilities of advanced electric propulsion systems and exotic propulsion technologies as (photonic) solar sail. This paper investigates minimum time optimal direct transfer scenarios for a mission to the circumsolar space, in which a solar electric propelled spacecraft enters an elliptical highly inclined orbit around the Sun with a perihelion radius of 0.3 AU (about 65 solar radii). A comparison of the performance between a solar electric and a solar sail propelled spacecraft in this high energy mission scenario, is also discussed.

Using an indirect approach, a number of time-optimal direct transfer trajectories have been simulated, and the resulting data have been collected in graphs and tables for a trade-off analysis of the main mission parameters. Taking into account the actual performance of an advanced electric propulsion system (the NASA Evolutionary Xenon Thruster), the simulations show that a spacecraft with an injected mass of 1000 kg reaches a target orbit of inclination 24 deg and aphelion radius 0.8 AU in about 2.6 years. In this mission scenario, the final spacecraft mass is slightly greater than the 56% of the injected mass. This rather small value could be increased, at the expense of an increased flight time, by including, in the performance index, a term depending on the final spacecraft mass. On the other hand, a transfer trajectory that minimizes only the propellant consumption, should be time-constrained. Therefore, the results of the minimum-time problem ensure that the time-constraint in a fuel-optimal problem is feasible. The use of optimal control theory has provided an optimal switching law for the operation point of the engine, showing substantially different behaviors depending on the available power. This situation can correspond to an intentionally undersized power system or to a partial failure.

A natural extension of the analysis discussed in this paper, is to explore the influence of the

launch C_3 on the flight time and required propellant mass through a sensitivity analysis. On the other hand, one or more gravity-assist maneuvers, whose aim is to reduce the propellant consumption as in the case of the ESA's Solar Orbiter mission study, can be included in the trajectory optimization process. However, a multiple gravity assist trajectory places additional constraints related to the planetary ephemerides, whereas a direct transfer offers a greater flexibility in the launch window selection.

Acknowledgments

The authors would like to acknowledge the valuable support and suggestions by Prof. Giovanni Mengali from University of Pisa, and Prof. Lorenzo Casalino from Politecnico di Torino.

References

APL Team, Solar Probe Plus mission engineering study report. The Johns Hopkins University Applied Physics Laboratory, available online (cited February 4, 2012) `http://solarprobe.jhuapl.edu/mission/docs/SolarProbeME.pdf`, March 2008.

Bate, R. R., Mueller, D. D., White, J. E., Fundamentals of Astrodynamics. Dover Publications, New York, p. 429, ISBN: 0-486-60061-0, 1971.

Betts, J. T., Survey of numerical methods for trajectory optimization. Journal of Guidance, Control, and Dynamics 21 (2), 193–207, doi: 10.2514/2.4231, March-April 1998.

Betts, J. T., Very low-thrust trajectory optimization using a direct SQP method. Journal of Computational and Applied Mathematics 120 (1), 27–40, doi: 10.1016/S0377-0427(00)00301-0, August 2000.

Brophy, J. R., Noca, M., Electric propulsion for Solar System exploration. Journal of Propulsion and Power 14 (5), 700–707, doi: 10.2514/2.5332, September-October 1998.

Bryson, A. E., Ho, Y. C., Applied Optimal Control. Hemisphere Publishing Corporation, New York, NY, Ch. 2, pp. 71–89, ISBN: 0-891-16228-3, 1975.

Casalino, L., Colasurdo, G., Pastrone, D., Optimization procedure for preliminary design of opposition-class Mars missions. Journal of Guidance, Control, and Dynamics 21 (1), 134–140, doi: 10.2514/2.4209, January-February 1998.

Casalino, L., Colasurdo, G., Pastrone, D., Optimal low-thrust escape trajectories using gravity assist. Journal of Guidance, Control, and Dynamics 22 (5), 637–642, doi: 10.2514/2.4451, September-October 1999.

Ceriotti, M., McInnes, C. R., Generation of Optimal Trajectories for Earth Hybrid Pole Sitters. Journal of Guidance, Control, and Dynamics 34 (3), 847–859, doi: 10.2514/1.50935, May-June 2011.

Chobotov, V. A., Orbital Mechanics, 2nd Edition. AIAA Education Series. American Institute of Aeronautics and Astronautics, New York, Ch. 9, ISBN: 1-563-47179-5, 1996.

Circi, C., Optimal strategy for geostationary orbit acquisition using ion propulsion. Journal of Guidance, Control, and Dynamics 26 (4), 608–614, doi: 10.2514/2.5088, July-August 2003.

Circi, C., Mars and Mercury missions using solar sails and solar electric propulsion. Journal of Guidance, Control, and Dynamics 27 (3), 496–498, doi: 10.2514/1.5425, May-June 2004.

Dachwald, B., Solar sail performance requirements for missions to the outer Solar System and beyond. In: 55^{th} International Astronautical Congress. Vancouver, Canada, paper IAC-04-S.P.11, 04–08 October 2004.

Dachwald, B., Optimal solar sail trajectories for missions to the outer Solar System. Journal of Guidance, Control, and Dynamics 28 (6), 1187–1193, doi: 10.2514/1.13301, November-December 2005.

Dachwald, B., Macdonald, M., McInnes, C. R., et al., Impact of optical degradation on solar sail mission performance. Journal of Spacecraft and Rockets 44 (4), 740–749, doi: 10.2514/1.21432, July-August 2007.

Dachwald, B., Mengali, G., Quarta, A. A., et al., Parametric model and optimal control of

solar sails with optical degradation. Journal of Guidance, Control, and Dynamics 29 (5), 1170–1178, doi: 10.2514/1.20313, September-October 2006a.

Dachwald, B., Ohndorf, A., Wie, B., Solar sail trajectory optimization for the solar polar imager (SPI) mission. In: AIAA/AAS Astrodynamics Specialist Conference and Exhibit. Keystone, Colorado, paper AIAA 2006-6177, August 21–24 2006b.

ESA Study Scientists. Solar orbiter: Exploring the Sun-heliosphere connection. Definition Study Report ESA/SRE(2011)14, European Space Agency, available online (cited February 4, 2012) `http://sci.esa.int/science-e/www/object/index.cfm?fobjectid=48985`, July 2011.

Heliophysics Roadmap Team. Heliophysics/solar & space physics of a new era: Recommended roadmap for science and technology 2009–2030. Report to the NASA Advisory Council Heliophysics Subcommittee, NASA, available online (cited February 23, 2012) `http://sec.gsfc.nasa.gov/2009_Roadmap.pdf`, May 2009.

Herman, D. A., Soulas, G. C., Patterson, M. J., NEXT long-duration test neutralizer performance and erosion characteristics. In: The 31st International Electric Propulsion Conference. University of Michigan, USA, paper IEPC-2009-154, September 20–24 2009.

Hoare, C. A. R., Quicksort. The Computer Journal 5 (1), 10–16, doi:10.1093/comjnl/5.1.10, 1962.

Johnson, L., Young, R., Alhorn, D., et al., Solar sail propulsion: Enabling new capabilities for heliophysics. Tech. Rep. M11-0117, NASA, available online (cited July 11, 2012) `http://hdl.handle.net/2060/20110007225`, 2010.

Leipold, M., Götz, M., Hybrid photonic/electric propulsion. Tech. Rep. SOL4-TR-KTH-0001, Kayser-Threde GmbH, Munich, Germany, ESA contract No. 15334/01/NL/PA, January 2002.

Macdonald, M., McInnes, C. R., Analytical control laws for planet-centered solar sailing. Journal of Guidance, Control, and Dynamics 28 (5), 1038–1048, doi: 10.2514/1.11400, September-October 2005.

Macdonald, M., Hughes, G. W., McInnes, C. R., et al., Solar Polar Orbiter: A Solar Sail Technology Reference Study . Journal of Spacecraft and Rockets 43 (5), 960–972, doi: 10.2514/1.16408, September-October 2006.

Macdonald, M., McInnes, C. R., Solar sail science mission applications and advancement. Advances in Space Research 48 (11), 1702–1716, doi: 10.1016/j.asr.2011.03.018, December 2011.

McInnes, C. R., Solar Sailing: Technology, Dynamics and Mission Applications. Springer-Praxis Series in Space Science and Technology. Springer-Verlag, Berlin, pp. 13–14, 1999.

Mengali, G., Quarta, A. A., Trajectory design with hybrid low-thrust propulsion system. Journal of Guidance, Control, and Dynamics 30 (2), 419–426, doi: 10.2514/1.22433, March-April 2007.

Mengali, G., Quarta, A. A., Rapid solar sail rendezvous missions to asteroid 99942 Apophis. Journal of Spacecraft and Rockets 46 (1), 134–140, doi: 10.2514/1.37141, January-February 2009.

Oh, D. Y., Evaluation of solar electric propulsion technologies for discovery-class missions. Journal of Spacecraft and Rockets 44 (2), 399–411, doi: 10.2514/1.21613, March-April 2007.

Oh, D. Y., Landau, D., Randolph, T., et al., Analysis of system margins on deep space missions using solar electric propulsion. In: 44th AIAA/ASME/SAE/ASEE Joint Propulsion Conference & Exhibit. Hartford, CT, paper AIAA 2008-5286, July 21–23 2008.

Patterson, M. J., Benson, S. W., NEXT ion propulsion system development status and performance. In: 43rd AIAA/ASME/SAE/ASEE Joint Propulsion Conference and Exhibit. Cincinnati, OH, paper AIAA 2007-5199, July 8–11 2007.

Patterson, M. J., Haag, T. W., Foster, J. E., et al., Development status of a 5/10-kW class ion engine. In: 37th AIAA/ASME/SAE/ASEE Joint Propulsion Conference and Exhibit. Salt Lake City, UT, paper AIAA 2001-3489, July 8–11 2001.

Quarta, A. A., Mengali, G., Minimum-time space missions with solar electric propulsion. Aerospace Science and Technology 15 (5), 381–392, doi: 10.1016/j.ast.2010.09.003, July-

August 2011.

Rayman, M. D., Williams, S. N., Design of the first interplanetary solar electric propulsion mission. Journal of Spacecraft and Rockets 39 (4), 589–595, doi: 10.2514/2.3848, July-August 2002.

Reckart, T. A. NASA's evolutionary xenon thruster (NEXT). NASA fact sheets, In-Space Propulsion Technology Project, John H. Glenn Research Center, Cleveland, Ohio 44135, availale online (cited February 6, 2012) `http://microgravity.grc.nasa.gov/Advanced/ScienceProject/FactSheets/NEXT.pdf`, May, 22 2009.

Saleh, J. H., Hastings, D. E., Newman, D. J., Spacecraft design lifetime. Journal of Spacecraft and Rockets 39 (2), 244–257, doi: 10.2514/2.3806, March-April 2002.

Sauer, Jr., C. G., Solar sail trajectories for solar polar and interstellar probe missions. In: AAS/AIAA Astrodynamics Specialist Conference. Girdwood, Alaska, paper AAS 99-336, 15–19 August 1999.

Shampine, L. F., Gordon, M. K., Computer Solution of Ordinary Differential Equations: The Initial Value Problem. W. H. Freeman & Co Ltd, San Francisco, Ch. 10, ISBN: 0-716-70461-7, June 1975.

Tsuda, Y., Mori, O., Funase, R., et al., Flight status of IKAROS deep space solar sail demonstrator. Acta Astronautica 69 (9-10), 833–840, doi: 10.1016/j.actaastro.2011.06.005, November-December 2011.

Van Noord, J., Lifetime assessment of the NEXT ion thruster. In: 43rd AIAA/ASME/SAE/ASEE Joint Propulsion Conference and Exhibit. Cincinnati, OH, paper AIAA 2007-5274, July 8–11 2007.

Vasile, M., Bernelli-Zazzera, F., Optimizing low-thrust and gravity assist maneuvers to design interplanetary trajectories. The Journal of the Astronautical Sciences 51 (1), 13–35 , January-March 2003a.

Vasile, M., Bernelli-Zazzera, F., Trajectory Design Combining Low-Thrust and Gravity Assist Manoeuvres. Vol. 79 of Operations Research in Space and Air. Springer, Ch. 12, pp. 1–31,

ISBN: 978-1-4020-1218-1, 2003b.

Walker, M. J. H., Owens, J., Ireland, B., A set of modified equinoctial orbit elements. Celestial Mechanics 36, 409–419, doi: 10.1007/BF01227493, August 1985.

Walker, M. J., Erratum - a set of modified equinoctial orbit elements. Celestial Mechanics 38 (4), 391–392, doi: 10.1007/BF01238929, April 1986.

Williams, S. N., Coverstone-Carroll, V., Benefits of solar electric propulsion for the next generation of planetary exploration missions. Journal of the Astronautical Sciences 45 (2), 143–159, April-June 1997.

List of Tables

m_0 [kg]	t_1 [days]	m_p/m_0	m_p [kg]	a_c [mm/s^2]	$\sigma_{\rm sa}$ [g/m^2]
550	509.7	0.4243	233.3	0.7727	5.01
600	550.2	0.4198	251.9	0.7236	5.29
650	601.7	0.4239	275.5	0.6888	5.61
700	658.6	0.4308	301.5	0.5800	6.77
750	712.8	0.4351	326.3	0.5180	7.66
800	749.9	0.4292	343.4	0.4953	7.90
850	793.2	0.4273	363.2	0.4722	8.25
900	843.4	0.4291	386.1	0.4606	8.49
950	902.9	0.4351	413.4	0.4321	9.18
1000	952.9	0.4363	436.2	0.3898	10.20
1050	998.1	0.4352	457.0	0.3752	10.57
1100	1031.2	0.4292	472.1	0.3656	10.70
1150	1080.7	0.4303	494.8	0.3571	10.99
1200	1135.6	0.4333	519.9	0.3265	12.10
1250	1187.0	0.4348	543.5	0.3151	12.58
1300	1240.1	0.4368	567.7	0.3081	12.93
1350	1307.4	0.4434	598.6	0.2828	14.29
1400	1319.2	0.4314	604	0.2808	14.01
1450	1371.7	0.4331	628.1	0.2723	14.50
1500	1432.8	0.4373	656	0.2659	15.00
1600	1511.1	0.4324	691.8	0.2454	16.07
1700	1612.4	0.4342	738.3	0.2338	16.93
1800	1720	0.4375	787.5	0.2163	18.44

Table 1
Mission performance as a function of the injected mass m_0 (with $P_\oplus = 10\,\mathrm{kW}$, $r_p = 0.3\,\mathrm{AU}$, $r_a = 0.8\,\mathrm{AU}$, and $i_1 = 24\,\mathrm{deg}$).

$P_\oplus$ [kW]	t_1 [days]	m_p/m_0	a_c [mm/s^2]	$\sigma_{\rm sa}$ [g/m^2]
5.5	1278.6	0.5125	0.2880	16.22
6	1134.7	0.4895	0.3267	13.66
6.5	1044.6	0.4713	0.3619	11.87
7	1004.6	0.46	0.3733	11.23
7.5	1003	0.4592	0.3737	11.20
8	987.2	0.4520	0.3786	10.88
8.5	964.8	0.4418	0.3858	10.44
9	959.7	0.4394	0.3875	10.34
9.5	952.9	0.4363	0.3898	10.20
10	952.9	0.4363	0.3898	10.20

Table 2
Mission performance as a function of the initial solar array output power $P_\oplus$ (with $m_0 = 1000\,\text{kg}$, $r_p = 0.3\,\text{AU}$, $r_a = 0.8\,\text{AU}$, and $i_1 = 24\,\text{deg}$).

i_1 [deg]	t_1 [days]	m_p/m_0	a_c [mm/s^2]	$\sigma_{\rm sa}$ [g/m^2]
0	673.4	0.3083	0.4058	6.92
5	693.6	0.3176	0.4015	7.21
10	732.9	0.3355	0.4355	7.02
15	788.3	0.3609	0.4015	8.19
20	873.9	0.4001	0.4034	9.04
25	965.8	0.4422	0.3924	10.27
30	1052.8	0.4820	0.4048	10.85

Table 3
Mission performance as a function of i_1 (with $m_0 = 1000\,\mathrm{kg}$, $P_\oplus = 10\,\mathrm{kW}$, $r_p = 0.3\,\mathrm{AU}$, and $r_a = 0.8\,\mathrm{AU}$).

r_a [AU]	t_1 [days]	m_p/m_0	a_c [mm/s^2]	$\sigma_{\rm sa}$ [g/m^2]
0.3	1240	0.5679	0.2614	19.81
0.4	1151.5	0.5272	0.2884	16.66
0.5	1078.6	0.4938	0.3179	14.16
0.6	1018.8	0.4665	0.3551	11.98
0.7	969.7	0.444	0.3756	10.78
0.8	952.9	0.4363	0.3898	10.20
0.9	914.5	0.4187	0.4108	9.29
1	893.5	0.4091	0.4260	8.75

Table 4
Mission performance as a function of r_a (with $m_0 = 1000\,\mathrm{kg}$, $P_\oplus = 10\,\mathrm{kW}$, $r_p = 0.3\,\mathrm{AU}$, and $i_1 = 24\,\mathrm{deg}$).

List of Figures

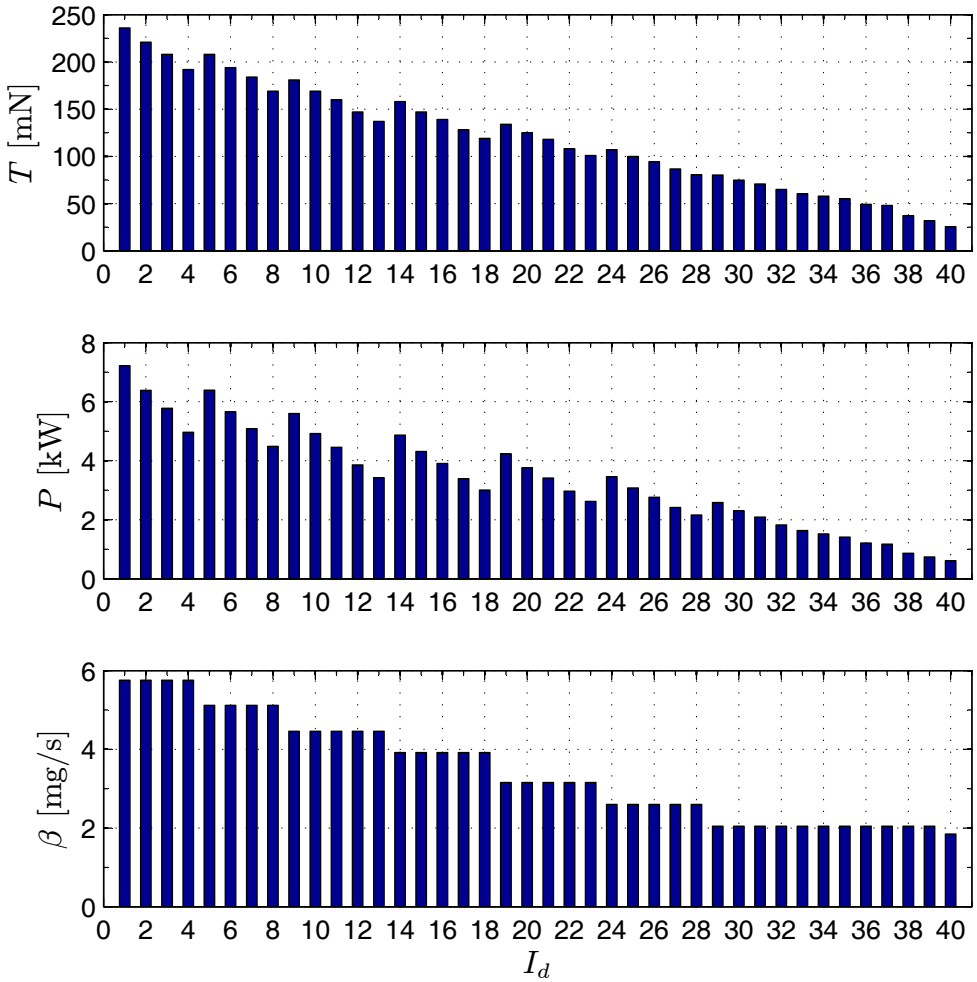

Figure 1. Propulsion system operation points in terms of thrust T, propellant mass flow rate β, and PPU input power P [data adapted from Patterson and Benson (2007)].

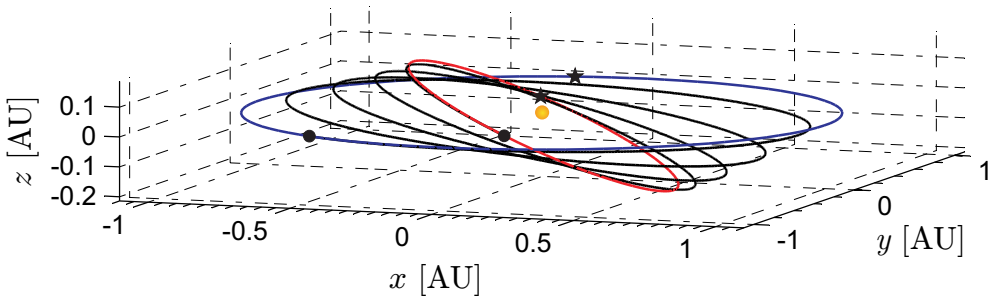

(a) Three-dimensional view.

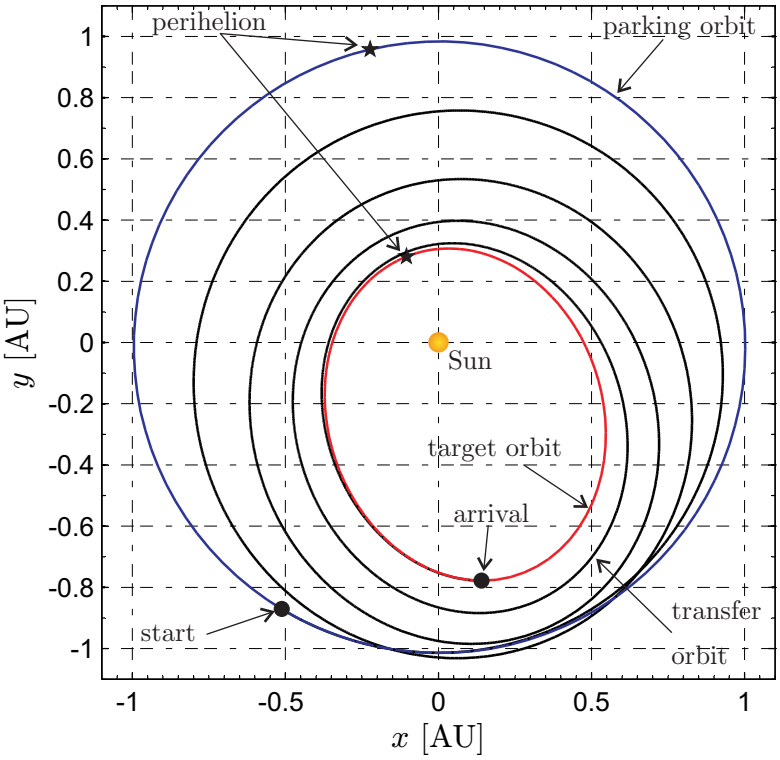

(b) Ecliptic projection.

Figure 2. Optimal transfer trajectory when $m_0 = 1000\,\mathrm{kg}$, $P_\oplus = 10\,\mathrm{kW}$, $r_p = 0.3\,\mathrm{AU}$, $r_a = 0.8\,\mathrm{AU}$, and $i_1 = 24\,\mathrm{deg}$.

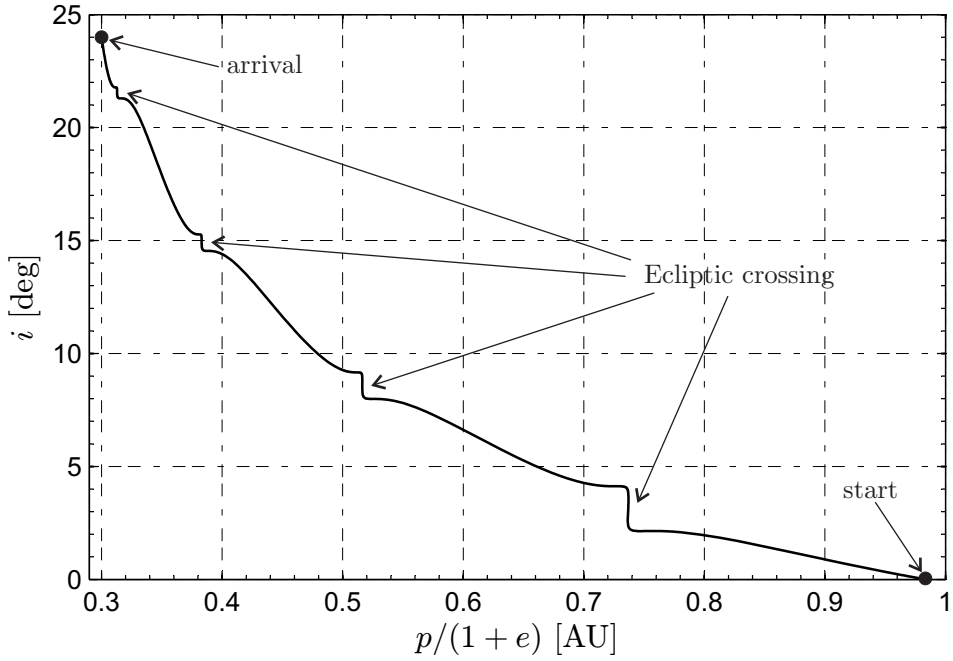

(a) Inclination vs. perihelion radius

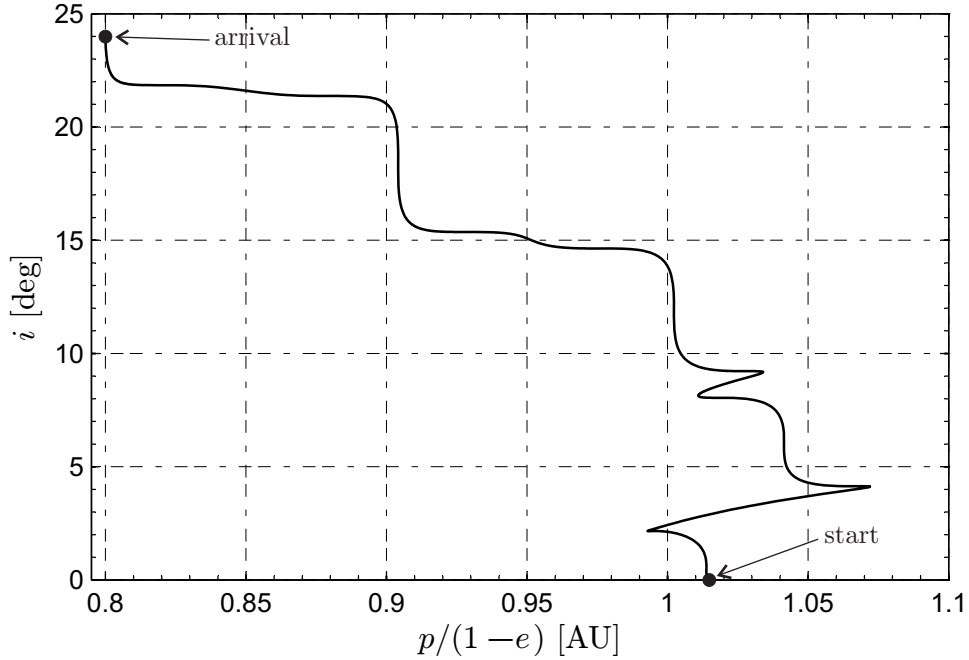

(b) Inclination vs. aphelion radius

Figure 3. Orbital inclination over perihelion and aphelion radius of the spacecraft osculating orbit ($m_0 = 1000\,\mathrm{kg}$ and $P_\oplus = 10\,\mathrm{kW}$, $r_p = 0.3\,\mathrm{AU}$, $r_a = 0.8\,\mathrm{AU}$ and $i_1 = 24\,\mathrm{deg}$).

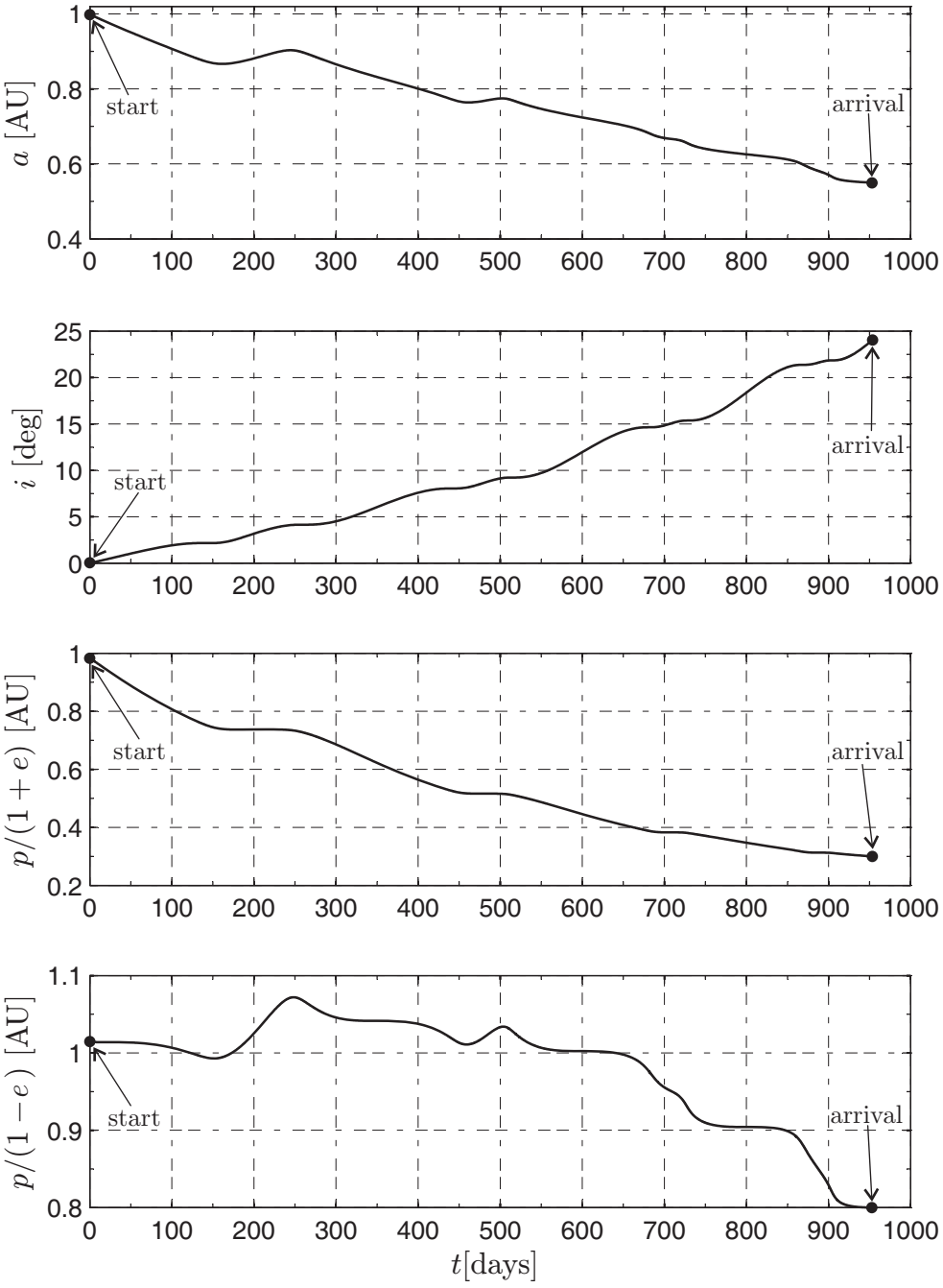

Figure 4. Time variation of the osculating orbit's semimajor axis, inclination, perihelion, and aphelion radius (with $m_0 = 1000\,\mathrm{kg}$, $P_\oplus = 10\,\mathrm{kW}$, $r_p = 0.3\,\mathrm{AU}$, $r_a = 0.8\,\mathrm{AU}$ and $i_1 = 24\,\mathrm{deg}$)

.

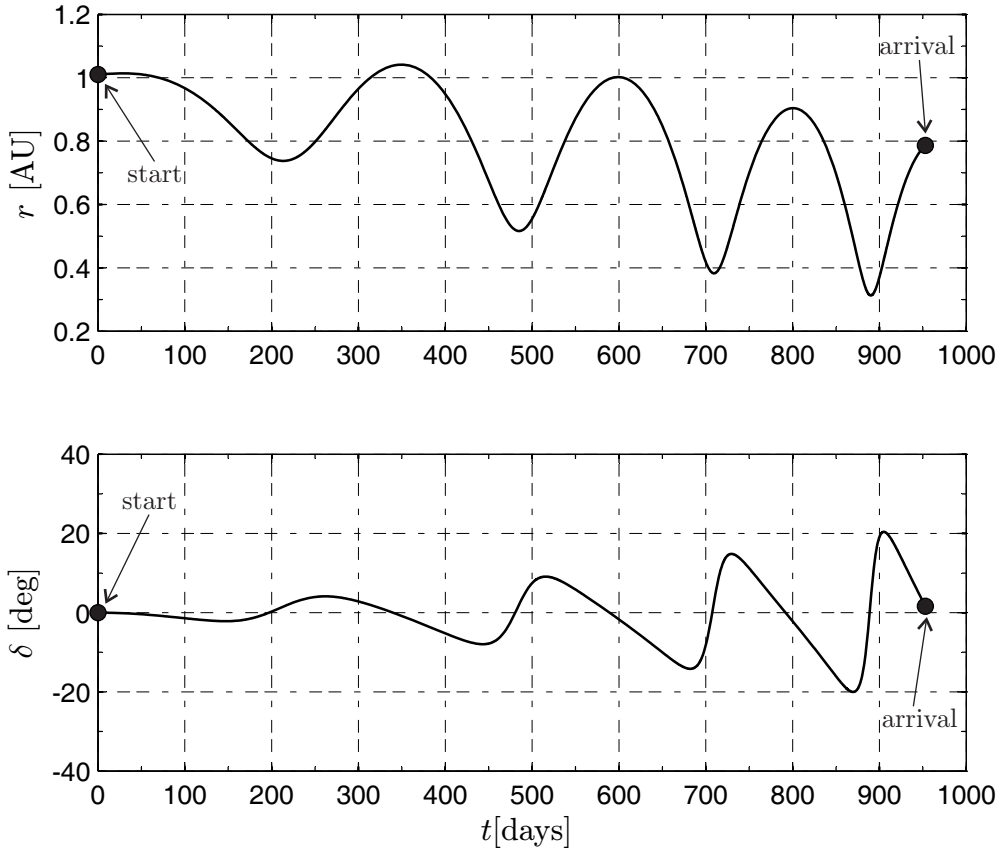

Figure 5. Sun-spacecraft distance r and ecliptic declination δ vs. time (with $m_0 = 1000\,\mathrm{kg}$, $P_\oplus = 10\,\mathrm{kW}$, $r_p = 0.3\,\mathrm{AU}$, and $r_a = 0.8\,\mathrm{AU}$).

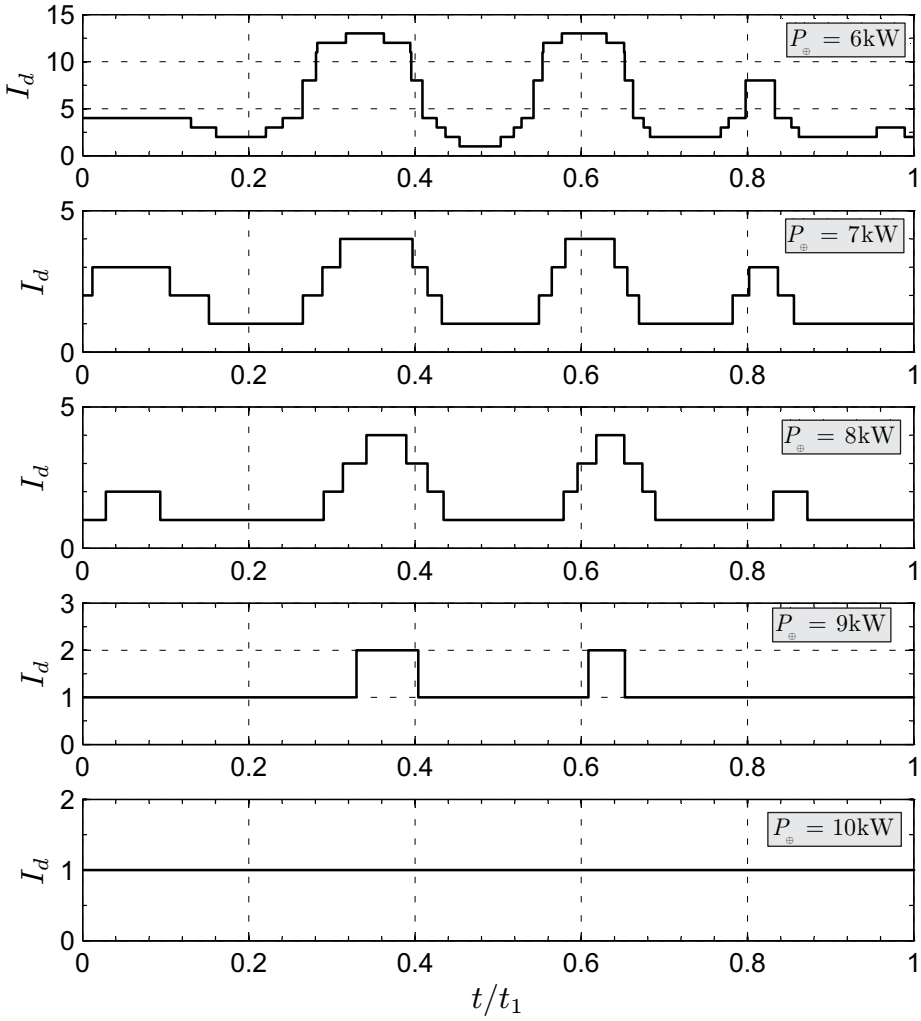

Figure 6. Thruster operation point I_d vs. time as a function of the initial solar array output power $P_\oplus$ (with $m_0 = 1000\,\mathrm{kg}$, $r_p = 0.3\,\mathrm{AU}$, $r_a = 0.8\,\mathrm{AU}$, and $i_1 = 24\,\mathrm{deg}$).

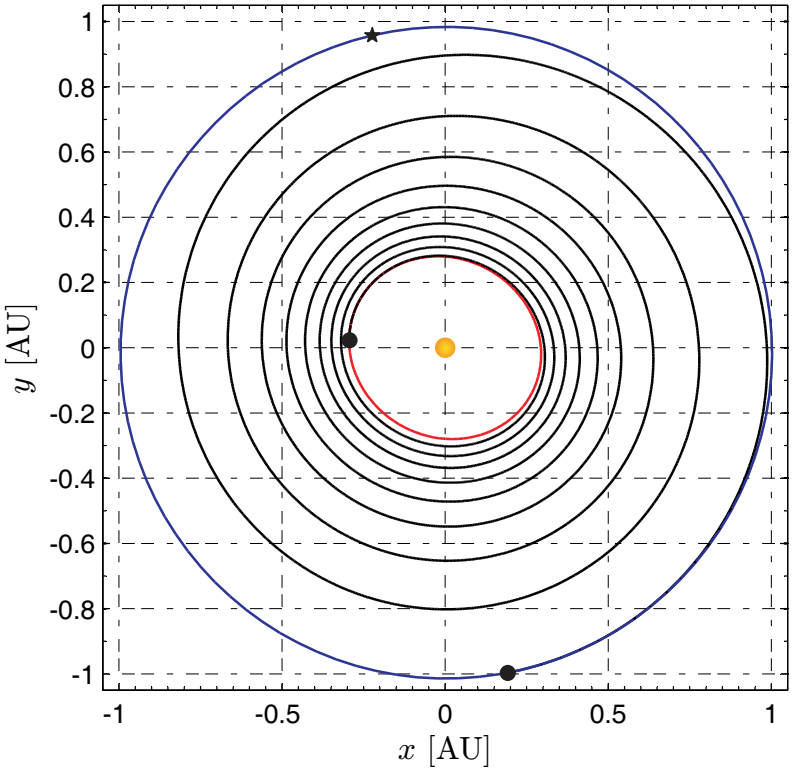

Figure 7. Ecliptic projection of the optimal transfer trajectory when $m_0 = 1000\,\mathrm{kg}$, $P_\oplus = 10\,\mathrm{kW}$, $r_p \equiv r_a = 0.3\,\mathrm{AU}$, and $i_1 = 24\,\mathrm{deg}$.